Journal of Civil Structural Health Monitoring (2022) 12:537–556
https://doi.org/10.1007/s13349-022-00563-7

ORIGINAL PAPER

A pilot project for the long-term structural health monitoring of historic city gates

Giacomo Zini[1] · Michele Betti[1] · Gianni Bartoli[1]

Received: 18 October 2021 / Revised: 9 February 2022 / Accepted: 3 March 2022 / Published online: 23 March 2022

Abstract
This paper reports on a pilot project for long-term structural health monitoring of historical city gates. This structural typology is what today remains of the defensive structures that characterised the medieval centres of many European cities. Even though in the last years the scientific community has paid great attention to the structural analysis and on the structural health monitoring of masonry towers, which are apparently similar to the typology of city gates, only a few studies explicitly approach such heritage buildings. In most cases, the surviving gates are immersed in the daily vehicular-traffic flows and hence continuously subjected to traffic-induced vibration. Consequently, a key point both for their conservation is the assessment of the optimal sensors position to be used for reliable structural health monitoring procedures. These issues are here discussed with reference to a specific case: the San Niccolò gate in Florence (Italy). First, an expeditious experimental campaign performed with a reduced number of accelerometers is reported. This test is aimed to identify a numerical model that is subsequently employed to design the optimal sensor position of long-term structural monitoring. This optimal sensor grid must be assessed to ensure a low-cost and sustainable dynamic monitoring system but, at the same time, to maximize the information contents.

Keywords Historical city gate · Structural health monitoring (SHM) · Operational modal analysis (OMA) · Optimal sensor position (OSP) · Fisher information matrix (FIM)

1 Introduction

Historic masonry towers are one of the most widespread typologies of heritage buildings in Europe. Since the Middle Ages, towers were built for different aims: (1) as defensive and sighting points, (2) as a private house to represent the power of the owner's family, and (3) to manage the working day of the farmers with the bell sound (bell-towers). Due to their relevance as Cultural Heritage (CH) buildings, and considering their intrinsic vulnerability under horizontal dynamic loads, these structures have become in the last decades one of the main focuses among the scientific community. Thus, many scientific papers are nowadays available that discuss their vulnerability against seismic loads (e.g. [1–4]) or against the dynamic loads induced by the swinging of bells (e.g. [5–7]).

In the last years, a renewed attention of the international scientific community on the structural analysis of this typology of heritage building has been growing again, driven by technological advances. For instance, the recent developments of micro-electro-mechanical systems allow the use of low-cost and small-size sensors for continuous monitoring of such structures [8–10]. Meanwhile, it is possible to combine the results of a continuous dynamic monitoring system with sophisticated numerical finite element (FE) models for damage assessment and structural health monitoring purposes [11–17]. This process has been also fostered by the implementation of several Automated Operational Modal Analysis (A-OMA) procedures, aiming at the real time extraction of the modal properties from the dynamic signatures collected in serviceability conditions [13, 17–19]. As a consequence,

✉ Giacomo Zini
giacomo.zini@unifi.it

Michele Betti
michele.betti@unifi.it

Gianni Bartoli
gianni.bartoli@unifi.it

[1] Department of Civil and Environmental Engineering, University of Florence, Via di S. Marta 3, 50139 Florence, Italy

updating of FE models combined with dynamic results is widely adopted for masonry towers and bell-towers [20].

However, by analysing the scientific literature it is also possible to observe a lack of technical papers discussing the assessment of old city gates. To date, only a few studies, to the best authors' knowledge, approach such structural typology [21, 22]. This CH typology is what today remains of many of the defensive structures (the city walls) that characterised the medieval centres of many European cities. In the modern era, to obtain new spaces for the urban expansion of the old towns, many of these cities saw the demolition of their historic walls leaving in some cases only the city gates. This is for instance the case of the city centre of Florence (Italy). In 1865, the architect G. Poggi was commissioned to draw up the new urban plan for the city, and Poggi's plan included, among other developments, the demolition of the city walls and the creation of ring roads to manage the increasing demand for faster transportation vectors. As a result, the surviving gates are today immersed in the vehicular traffic flowing on such ring roads and continuously subjected to traffic-induced vibration [23–26].

This study, presenting the results obtained with a dynamic testing campaign performed on one of these survived city gates, is intended as a pilot project to design and set-up a reliable (i.e. able to minimize the maintenance costs, guaranteeing meantime a good efficiency) Structural Health Monitoring (SHM) framework for these structures. As a matter of fact, the design of this SHM system should combines the preservation needs, which characterize this kind of buildings, with the efficiency of the installed monitoring system.

From the one hand, to assure a reduced impact on the structure, a reduced number of sensors must be considered to avoid the set-up of invasive monitoring systems. In addition, such a reduced layout may solve the operational drawbacks due to the management of the large amount of data collected with a long-term dynamic monitoring systems [9, 10, 21]. From the other hand, this reduced number of sensors should be properly selected to identify the modal properties of the structure with a good resolution. Usually, frequencies can be estimated with a high degree of accuracy even when using sparse sensor grids (as shown in the automated procedures for the modal parameters identification recently proposed by several authors [18, 19, 27, 28]), but since these quantities are ambient-sensitive global indicators, they may fail to provide damage localization. Hence the sensor layout should be designed in order that the data obtained through Ambient Vibration Tests (AVT) on the sparse sensor grids is accurate enough to allow mode shapes reconstruction. This mean that the design of an optimal sensor layout (both number and positioning of sensors) capable to maximize the information for SHM should be performed with rational approaches able to qualify and quantify the information provided by the choice of sensor grid.

The paper first reports a brief description of the investigated city gate, together with the dynamic test campaign performed to identify its dynamic behaviour. To minimize the impact on the structure, the tests were performed with a reduced number of accelerometers. Subsequently, an optimization procedure based on Genetic Algorithms (GA) was used for the calibration of a FE model of this gate, and the identified FE model was eventually employed as a digital laboratory to optimize number and position of the sensors to be employed for long-term monitoring purpose. By applying a Gaussian white noise, the response of the gate was simulated and potentially recorded with a dense grid of sensors (the number of the sensors is equal to the dofs of the model). Eventually, the Optimal Sensor Position (OSP) was evaluated with an algorithm aiming to maximize the information contents of sensors by maximizing the Fisher Information Matrix (FIM) and, meantime, minimizing the redundancy between the information matrices of the sensors.

This paper is organized as follows: Sect. 2 briefly summarizes the research aim of this pilot study reporting on the workflow proposed to optimize the sensor layout to be employed for long-term SHM framework. Section 3 introduces a description of the city gates of Florence and reports a structural description of the one here considered (the San Niccolò gate). The experimental dynamic tests performed, and the modal identification of the structure, are summarized in Sect. 4. Section 5 discusses the FE model and its calibration based on the experimental results through a GA-based procedure. The identified FE model is then employed in Sect. 6 to simulate the AV response of the city tower over a dense sensor grid. Eventually, the algorithm employed to assess the OSP is reported in Sect. 7.

2 Research aim

This paper aims to introduce a pilot project for the design of the sensor layout of a long-term SHM for historic city gates reporting the case of Florence (Italy). While dynamic monitoring has been widely recognized as a powerful tool for SHM since the Eighties, still several issues remain open for its spread in the operative field for CH buildings. Among these, a key point is the OSP (both in terms of number and position of the sensors) to ensure a low-cost and sustainable long-term dynamic monitoring. This study proposes to tackle this issue for historic city gates through the workflow illustrated in Fig. 1. Once the case is selected, a fast OMA is performed to identify the main resonant frequencies. Then, a FE model of the structure is tuned to fit the experimental dynamic, as identified in the previous step, and employed to generate AV simulated responses. Assuming these responses as signals collected in a possible sensor layout, the OSP is next tackled introducing a hybrid method that allows

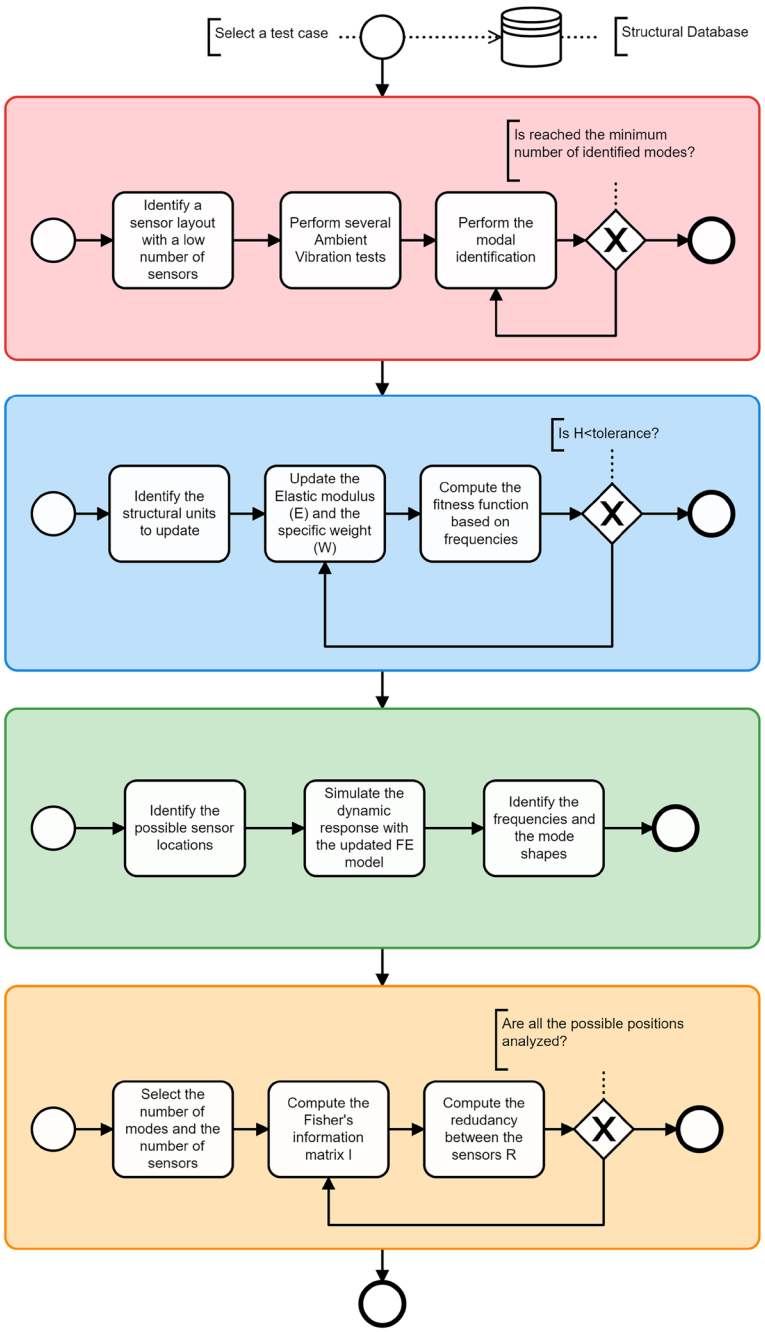

Fig. 1 Workflow of the proposed methodology, each sub-process box represents the following phases: (i) Fast AVT (red), (ii) FE model updating (blue), (iii) Simulated AVT (green) and (iv) OSP (yellow) (colour figure online)

maximization of the FIM and the minimization of the sensor redundancy. To check the effectiveness of the OSP, the mode shapes are backward compared with those obtained by the FE model by introducing a coherence index.

3 Historic city gates

In 1870, Architect G. Poggi started the demolition of the major part of the medieval Florentine walls to allow the construction of large ring roads. This intervention was part of a wider project, aimed at renewing the urban area of Florence just became the Capital of the newly born Italian State. After 150 years, Florence is no longer the Italian Capital, but the Poggi's ring roads are still there and some of the old city gates can be still observed. From the original 21 city gates of the medieval walls, 12 of them can be found around the city centre. In Fig. 2 is reported a picture of each gate, where some differences in the geometry can be directly observed (the materials and the construction techniques are approximatively the same). Some of these differences are due to the demolition of the upper levels

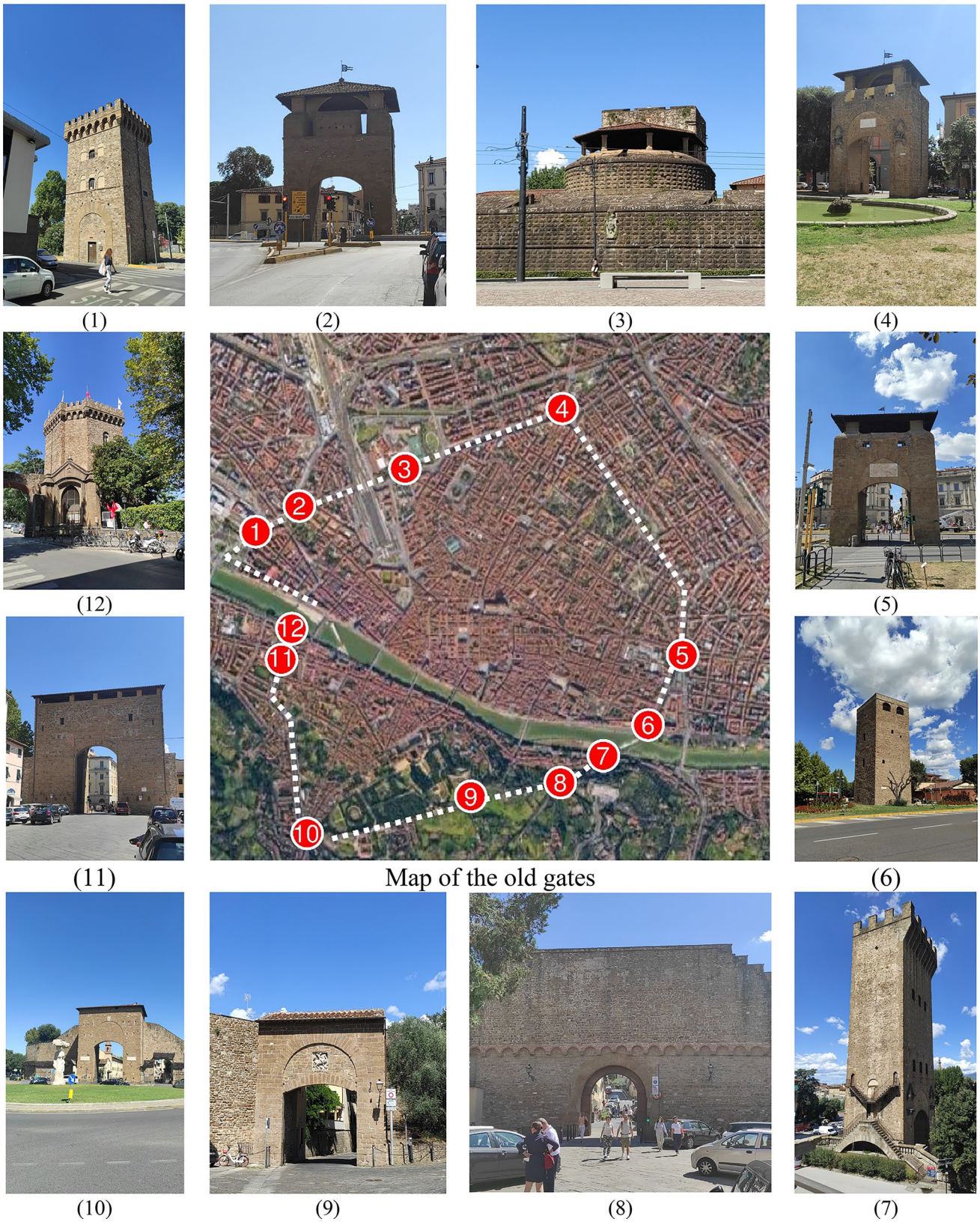

Fig. 2 The 12 Florentine's old-city gates and their location along with the medieval defensive walls [(1) Torre della Serpe; (2) Porta al Prato; (3) Porta a Faenza; (4) Porta San Gallo; (5) Porta alla croce; (6) Torre della zecca; (7) Porta San Niccolò; (8) Porta San Miniato; (9) Porta San Giorgio; (10) Porta Romana; (11) Porta San Frediano; (12) Torrino di Santa rosa]

made in the XVI century to increase their strength against cannon attacks.

Nowadays these survived gates are constantly subjected to traffic-induced vibrations that can speed up material degradation. Consequently, the definition of reliable SHM procedures is a key point both for their conservation and for avoiding injuries to people. In fact, almost under all the city gates pedestrian traffic is allowed, and in some cases vehicular traffic is allowed too (city gates N. 9, 10, 11 and 12; Fig. 2). To discuss a pilot project for the SHM of these structures, this paper specifically investigates the case study of San Niccolò city gate (N. 7 in Fig. 2).

3.1 San Niccolò city gate

The San Niccolò city gate is located along the Arno River in the South-East sector of the medieval city defensive walls. The Gate, built in 1324 following the design by Andrea Orcagna, is the only one that was not lowered during the XVI century. In 1875 a system of stairs was added on one side of the tower under the design of Architect Poggi. In 1933 the gate was strengthened with several steel chains at different levels, and the merlons at the top level were rebuilt as it is supposed they were in the medieval era.

The gate has a rectangular plan (about 10×15 m) and an overall height of about 42 m. Inside the gate, there are two wooden levels, each sustained by three masonry arches. From a structural point of view, the gate can be divided into three main macro-elements: (1) the double-thick masonry wall system, (2) the arches used to support the wooden levels and (3) the continuous masonry facade which is only on the outer side (Fig. 3). These macro-elements are characterized by similar material properties, and constructive techniques, and represent the homogeneous element whose stiffness has to be calibrated in the FE model updating procedure.

From the dynamic point of view, the continuous masonry façade, which is only on the outer side, corresponds to a C-shaped section for the structure. This aspect, combined with the large opening at the ground level, significantly differentiates the dynamic behaviour of the gate from the case of the masonry towers widely analysed in scientific literature.

To build the FE model of the gate, the FE code ANSYS was used. This numerical model was built with the available geometric data, paying specific attention to the correct reproduction of the macro-elements mentioned above. All these components were modelled by means of 3D solid 8-nodes isoparametric finite elements (SOLID185), having three degrees of freedom at each node, using a macro-modelling approach [29, 30]. The structure was modelled by assuming fixed restraints at the base, and the masonry was modelled as an isotropic linear elastic material being the FE model used to perform linear modal analyses.

The final 3D FE model, built as detailed as needed to represent the overall spatial configuration of masses and stiffness, consisted of 25,123 joints and 75,943 elements, corresponding to 74,565 degrees of freedom. Among the methods provided by ANSYS to compute natural frequencies and vibration modes, the block Lanczos algorithm was used. After tuning, the FE model was employed to optimize number and position of sensors to be employed for long-term monitoring. The 3D CAD view of the gate used to build the mesh of FE model is illustrated in Fig. 3c.

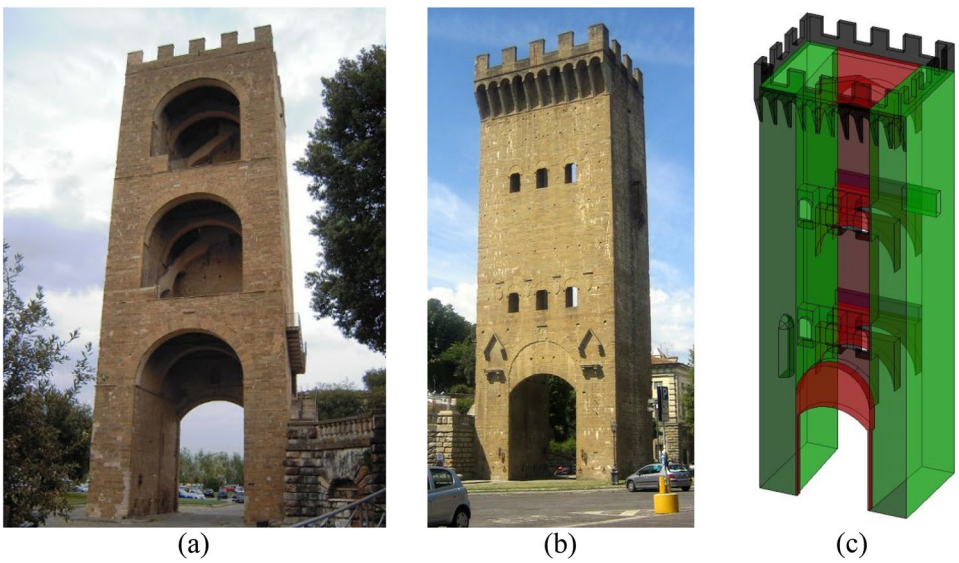

Fig. 3 **a** Inner and outer (**b**) view of the S. Niccolò gate, and 3D CAD geometric model (**c**)

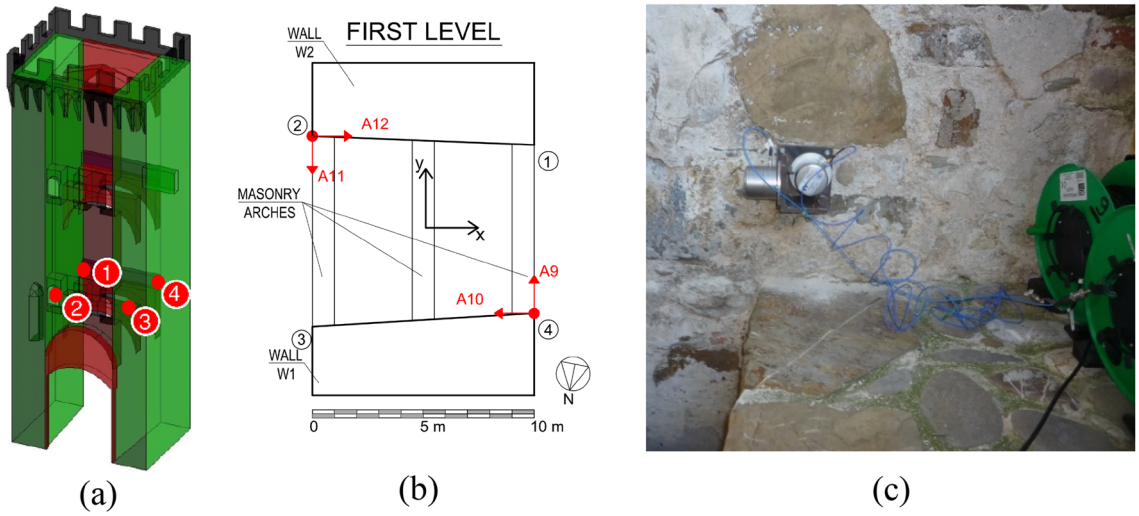

Fig. 4 **a**, **b** The measurement layout adopted in the AVT and **c** The piezoelectric accelerometers mounted in position 4

Table 1 Test performed during the experimental campaign on the San Niccolò gate

Test	Sampling rate (Hz)	Length (s)	Date (d/m/y)	Time (hh:mm)	Loads
NICC#02	400	2219	6/12/2016	11:48	AVT
NICC#03	400	1205	6/12/2016	12:30	AVT
NICC#04	400	1230	6/12/2016	12:57	AVT
NICC#06	400	1226	6/12/2016	13:50	AVT
NICC#07	400	1203	6/12/2016	14:13	AVT
NICC#23	400	1203	7/12/2016	11:01	AVT

4 Ambient vibration tests

To obtain a fast screen of the structural dynamic, the testing campaign was performed by using a reduced sensor layout: only four accelerometers (PCB-393B31 with a sensitivity of 10 V/g and a range of 0.5 g) were installed on the two corners of a level of the gate. Due to some constraints related to the electrical connections, it was not possible to record the top level of the gate and the investigated level was the one shown in Fig. 4.

The AVT were carried out to fully characterize the structural dynamics of the gate over two days of experimental investigation; few information about some selected tests is listed in Table 1.

The collected signals were filtered between 0.5 and 20 Hz with a third-order Butterworth filter and then resampled to 50 Hz to investigate the frequency band where the structural modes are expected to be. In this respect, simplified empirical and/or semi-analytical formulations for the estimation of the main frequencies of masonry towers were preliminarily considered. These formulations, together with the estimated frequency values, are summarized in Table 2. The obtained frequencies vary from 1.19 Hz [35] to 2.05 Hz [33], thus denoting a significant scattering provided by the current empirical or semi-empirical formulas.

Table 2 Empirical and/or semi-analytical formulations proposed for the estimation of the natural frequency of towers

References	Eqn	f_{NS}	f_{EW}
NTC [31]	$f_1 = \frac{1}{0.050H^{3/4}}$	1.225	=
Faccio et al. [32]	$f_1 = \frac{1}{0.0187H}$	1.292	=
NCSE [33]	$f_1 = \frac{\sqrt{L}}{0.06H\sqrt{\frac{H}{2L+H}}}$	1.591	2.048
Rainieri and Fabbrocino [34]	$f_1 = \frac{1}{0.0113H^{1.138}}$	1.279	=
Shakya et al. [35]	$f_1 = \frac{1}{0.0151H^{1.08}}$	1.188	=
Shakya et al. [35]	$f_1 = \frac{L^{0.17}}{0.03H\left(\frac{H}{L+H}\right)^{0.5}}$	1.341	1.489
Shakya et al. [35]	$f_1 = 3.58\left(\frac{H}{B}\right)^{-0.57}$	1.629	=
Bartoli et al. [36]	$f_1 \cong \frac{0.2a}{H_{eff}^2}(1-n)v_p$	n.a	1.644
Bartoli et al. [36]	$f_1 \cong \frac{0.15a}{H_{eff}^2}v_p$	n.a	1.608

Due to the low level of vibration recorded during the tests (the considered city gate is in an area where the vehicular traffic is limited), time and frequency domain techniques were used to compare the results and to obtain a robust modal identification. The Frequency Domain Decomposition (FDD) allowed to recognize several peaks in the singular values decomposition of the Power Spectral Density (PSD) matrix (Fig. 5). The first two modes are very close, thus a unique peak is visible in the first singular value of the PSD. However, the analysis of the

second singular value allows to clearly recognize the second resonant frequency.

The results obtained with the FFD were confirmed by the Stochastic Subspace Identification (SSI-cov) algorithm fed with the signals covariances: several alignments of stable poles in the stabilization chart are clearly visible (Fig. 6) that corresponds to the values provided by the FFD technique. In addition, the analysis of the data with the SSI-cov procedure allowed the identification of the first two modes that were now clearly separated.

The modal identification results for both techniques are summarized in Table 3, while the first six identified mode shapes are illustrated in Fig. 7. Due to the reduced sensor layout adopted for the expeditious testing campaign higher modes are poorly represented.

If the experimental results are compared with those provided by the simplified formulations reported in Table 2, it is possible to observe that the simplified one-parameter formulations commonly employed for masonry towers fail: they provide an estimation between 1.19 and 2.05 Hz against the experimental

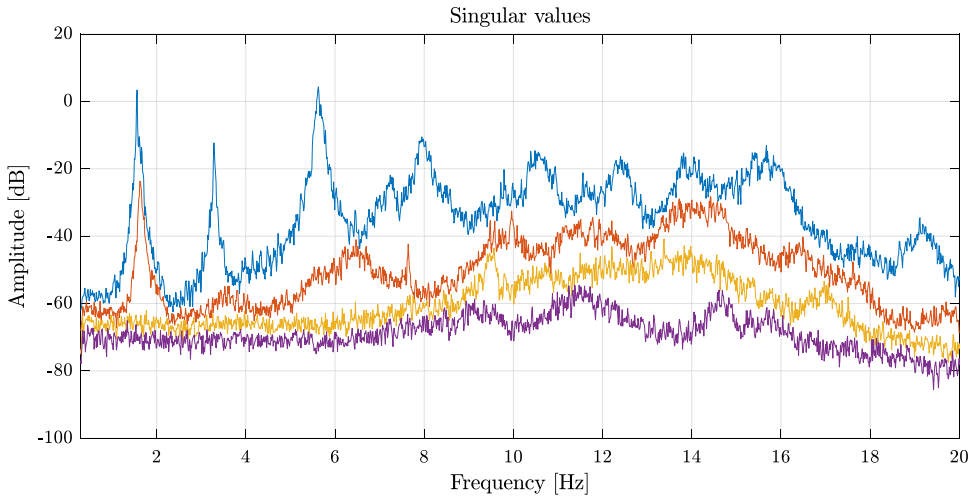

Fig. 5 The singular values of the PSD matrix during AVT

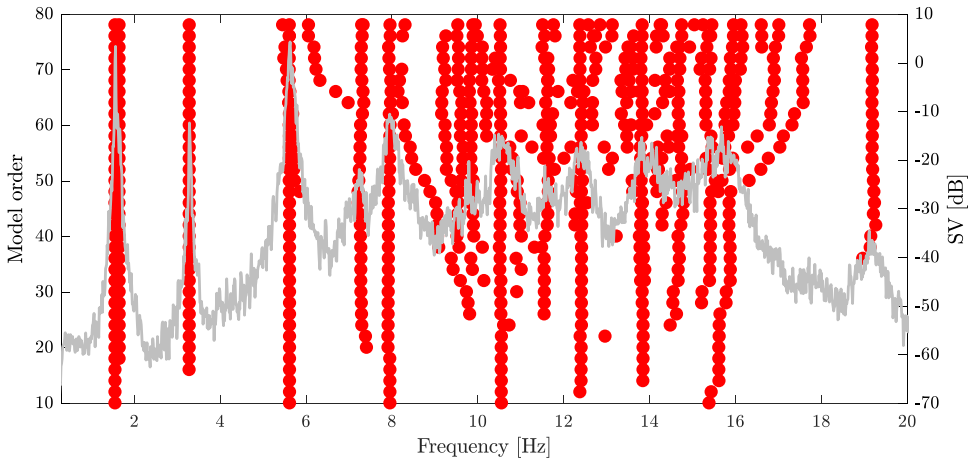

Fig. 6 The stabilization chart obtained with the SSI-cov technique during the AVTs

Table 3 Modes identified with the SSI-cov and the FDD (and comparison with tuned FE model)

Mode	Description	SSI-cov		FDD	Updated FE model (Hz)	Simulated AVT (Hz)
		$\mu(f_n)$ (Hz)	$\mu(\xi_n)$ (%)	f_n (Hz)		
TN#1	First bending NS	1.565 ± 0.0002	1.070 ± 0.050	1.566 ± 0.003	1.56	1.55
TN#2	First bending EW	1.661 ± 0.001	1.612 ± 0.234	1.630 ± 0.003	1.64	1.64
TN#3	First torsional	3.294 ± 0.001	0.948 ± 0.042	3.284 ± 0.003	3.22	3.20
TN#4	Second bending NS	5.629 ± 0.015	1.980 ± 0.064	5.612 ± 0.003	5.74	5.66
TN#5	Second bending EW	7.979 ± 0.032	2.230 ± 0.227	7.974 ± 0.003	8.05	8.14
TN#6	Second torsional	10.544 ± 0.021	2.320 ± 0.279	10.510 ± 0.003	10.37	–

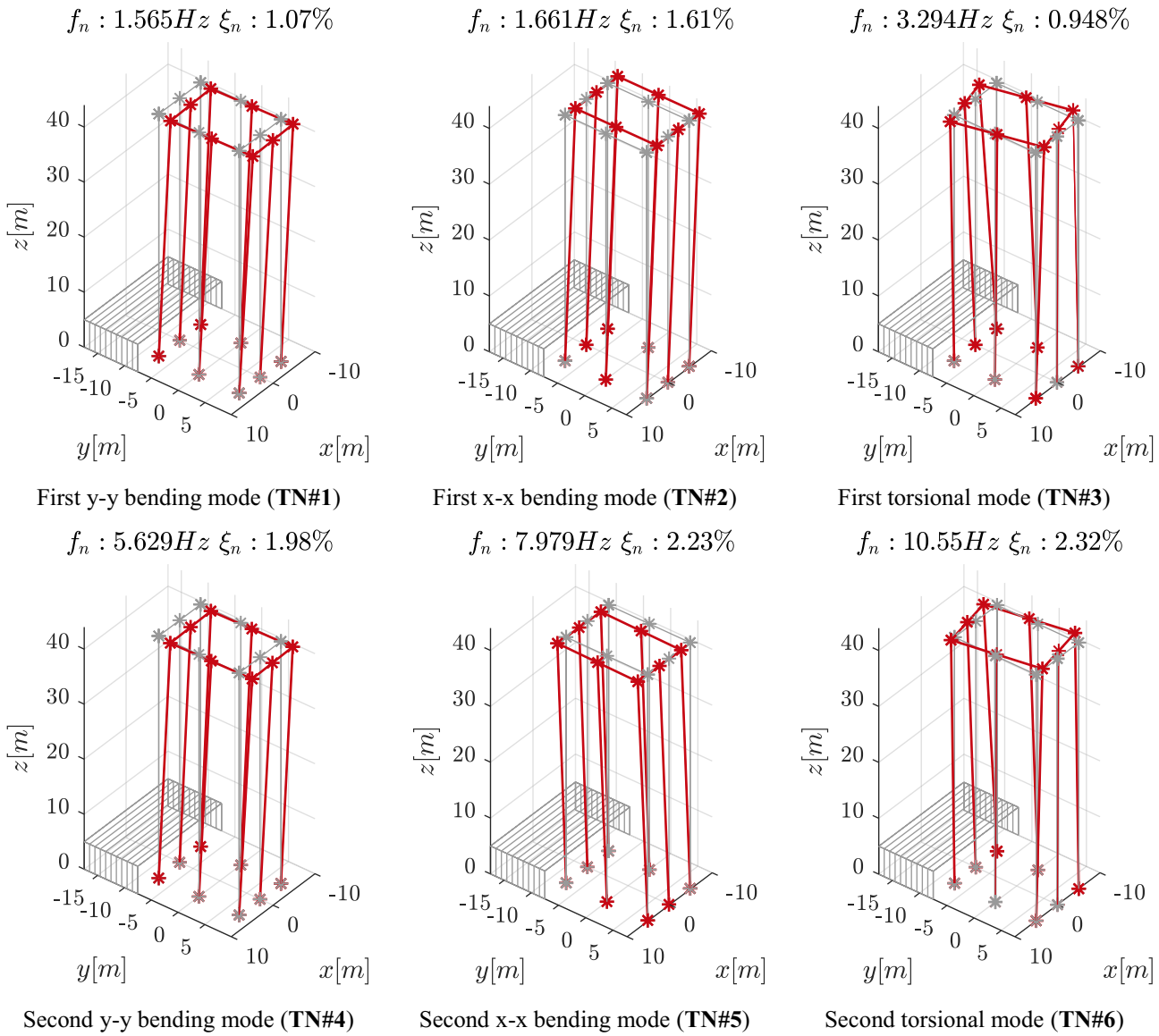

Fig. 7 The first six modes identified with the SSI-cov technique

values of 1.5–1.6 Hz. This difference highlight that even if historic city gates are commonly considered as a subset of the class of the masonry towers, their dynamic behaviour shows some significant differences that should be accounted for.

5 FE Model updating

The results of the expeditious experimental campaign were employed to identify a FE model of the city gate. The tuning of the FE model can be seen as an inverse problem where a parameterized numerical model is combined with an optimization algorithm which is employed to minimize an objective function that measures the differences between the numerical results and the measured data. FE model updating is hence a process where selected physical parameters of the FE model are gradually updated in such a way that the response of the FE model progressively approaches that of the real structure [37]. Due to the well-known problems of non-uniqueness and ill-conditioning of this procedure, the correct choice of the optimization algorithm is a key element to be considered to ensure a successful model updating.

In this respect, the efficiency of artificial intelligence algorithms such as the genetic algorithm (GA), originally introduced in the sixties by Holland [38] based on Darwin's principle of natural selection, has been demonstrated in the last decades. Being the GA a robust global optimization technique, it has been successfully applied in a plethora of minimization problems, involving mainly damage assessment, by many researchers since the early nineties [39–44]. It operates starting with

an initial population whose individuals, named chromosomes, are subjected to the operations inspired by the genetics laws. Individuals are selected according to their fitness performance, and they evolve based on genetic operations and replacement. Result of these operations, where the fitter chromosomes produce more offspring than the less fit ones, is a new population whose fitness is higher than the initial one [38].

The term chromosome refers to a candidate solution of the specific minimization problem, and the chromosome is composed of genes, each of which encodes specific data of the candidate solution. The standard GA involves four types of operators: (1) selection, (2) crossover, (3) mutation and (4) elitism. The purpose of the first operator is to selects the chromosomes in the population for reproduction: the most performing is the chromosome (i.e. higher its fitness value is), the more times it is likely to be selected for reproduction. The second operator generates two offspring by crossing, at a randomly chosen point, the parent chromosomes. Crossover implements the process of reproduction of natural selection. The third operator randomly replaces a gene in a chromosome with another one chosen from the solution space and has the purpose to introduce diversity in the solution process. The last operator, the elitism, transfers the best chromosomes of the current generation to the next generation.

Despite the proven efficiency of the GA algorithm, it should be remembered that several limitations still exist and among them it is possible to recall: (1) the problem of identifying a proper fitness function; (2) the premature convergence toward non-optimal solution (no general termination rules are available); (3) the proper choosing of the various parameters that characterize the algorithm (such as the size of the population, the mutation and the crossover rate, the elitism rate, and the selection methods, etc.).

Next, the coding of the GA-based model updating problem and the fitness function is reported.

5.1 Coding of the problem

The identification was performed selecting as updating parameters the modulus of elasticity (E) and the self-weight (W) of three macro-elements: (1) the double masonry wall system (MW); (2) the arches used to sustain the wooden levels (ARCH); and (3) the continuous masonry facade which is only on the outer side (MF). These components were selected to provide insight into the relative contribution of the stiffness of each component of the gate on the overall dynamic behaviour.

First identification analyses were performed where the self-weight was assumed varying between 18 kN/m^3 (lower value) and 22 kN/m^3 (upper value). Since these analyses converged toward a value of the self-weight between 18 and 19 kN/m^3, this was assumed as a fixed value and equal to 18 kN/m^3 for all the three macro-elements. Consequently, the final analyses were performed only varying the modulus of elasticity of the structural components (which is directly connected with the stiffness of the components). Its range of variation was assumed between 1500 MPa (lower value) and 9000 MPa (upper value) [45]. The Poisson coefficient was set equal to 0.2 for all the three macro-elements.

Chromosomes are so composed of 3 genes encoding the E of the three macro-elements, and genes can attain any real value between 0 (lower value of E) to 1 (upper value of E). Each chromosome represents a possible identified FE model whose eigenfrequencies (and eigenmodes) are numerically evaluated.

5.2 Fitness functions

The objective function was simply built by calculating the differences between experimental and numerical frequencies.

$$H_f(k) = \sum_{i=1}^{k} \left(\frac{f_{i,n} - f_{i,e}}{f_{i,e}} \right)^2 \tag{1}$$

In Eq. (1) k represents the number of identified frequencies employed for the tuning of the numerical model, and $f_{i,n}$ and $f_{i,e}$ denote the i-th numerical and experimental frequency (respectively).

To run the GA the parameters were chosen as follows: crossover was selected as 0.8, the mutation was set to 0.1 and elitism rate was chosen as 5% of the population. The gene numbers of each chromosome were 3, and the population size was chosen equal to 20 times the gene numbers. These values, which are problem dependent, were selected starting from suggestions in literature [39–41] and adapting them to the specific case. To perform the optimization, the ANSYS parametric APDL language was used to build the FE model in ASCII input form, whereas the code MATLAB was employed to apply the GA. In each iteration of the GA the chromosomes are generated according to the genetic rules above described, and then submitted to the ANSYS code to build the model and to obtain frequencies that are, in its turn, employed to evaluate the fitness of the population.

At the end of the process, the following values were attained: (1) $E_{\mathrm{MW}} = 7320$ MPa for the double masonry wall system; (2) $E_{\mathrm{ARCH}} = 5570$ MPa for the arches, and (3) $E_{\mathrm{MF}} = 3820$ MPa for the continuous masonry façade. The first mode of the updated numerical model is a spurious bending mode in the NS direction with a frequency of 1.56 Hz. The second mode shape is a bending mode in the EW direction with a frequency of 1.64 Hz. The third numerical mode shape has a frequency of 3.22 Hz and corresponds to a torsional mode-shape. The fourth mode shape is the upper bending mode in the NS direction and has a frequency of 5.74 Hz. The fifth mode shape, with a

frequency of 8.05 Hz, is a mode shape that involves the two masonry walls exhibiting mixed torsional-bending behaviour. Comparison between experimental and numerical frequencies is reported in Table 3, where it is possible to observe a quite good agreement between experimental and numerical frequencies. The numerical mode shapes are illustrated in Figs. 8 and 9. The analysis of the mode shapes highlights a specific behaviour of the city gate: its

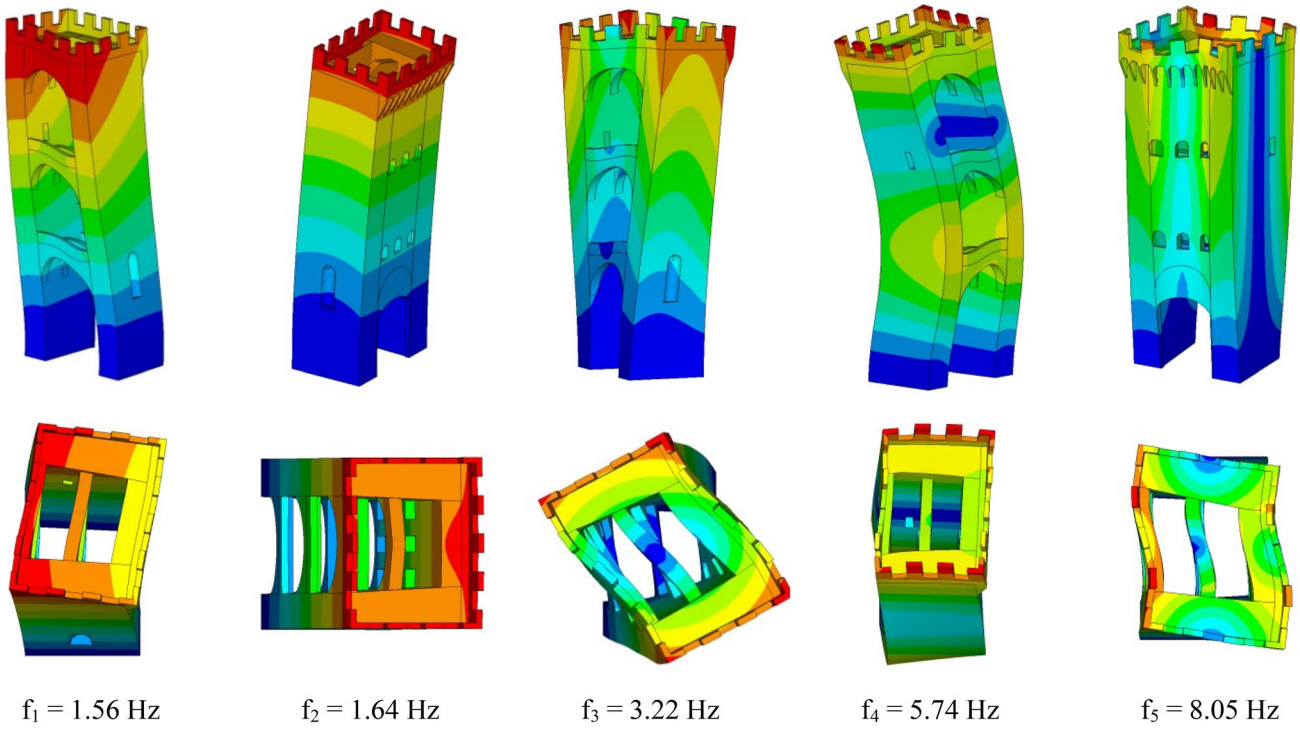

Fig. 8 View of the first 5 mode shapes (identified FE model)

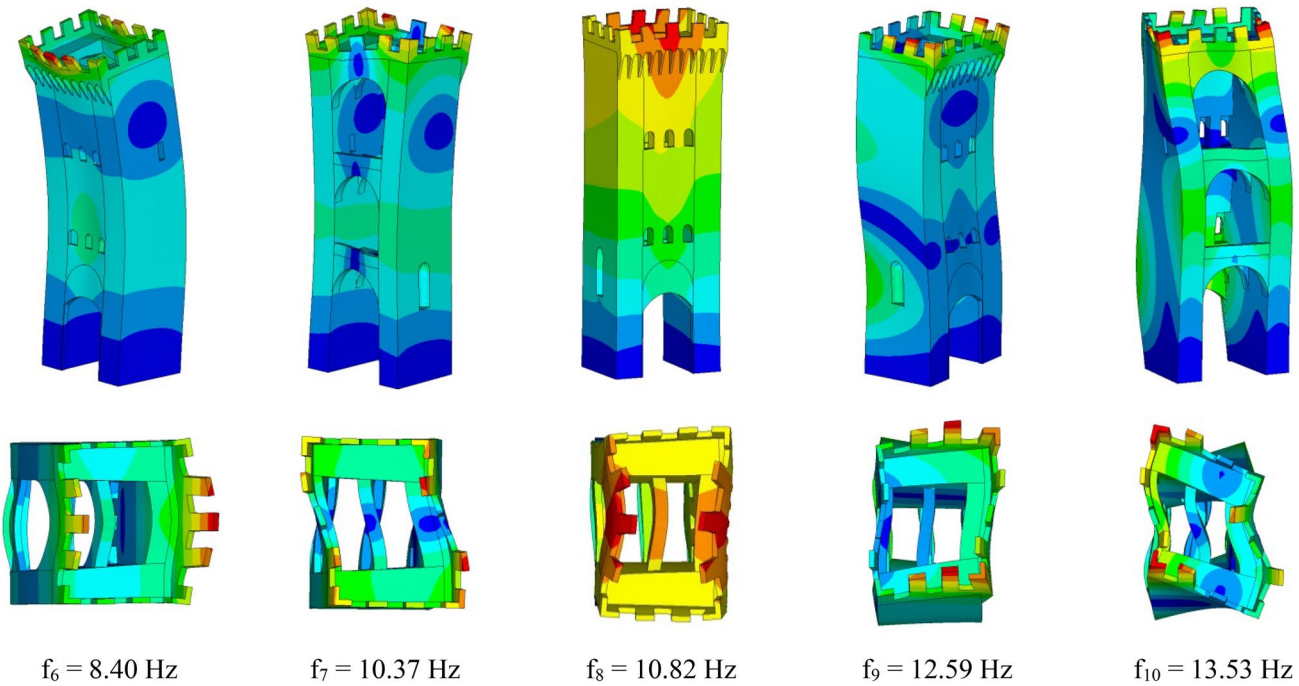

Fig. 9 View of the second 5 mode shapes (identified FE model)

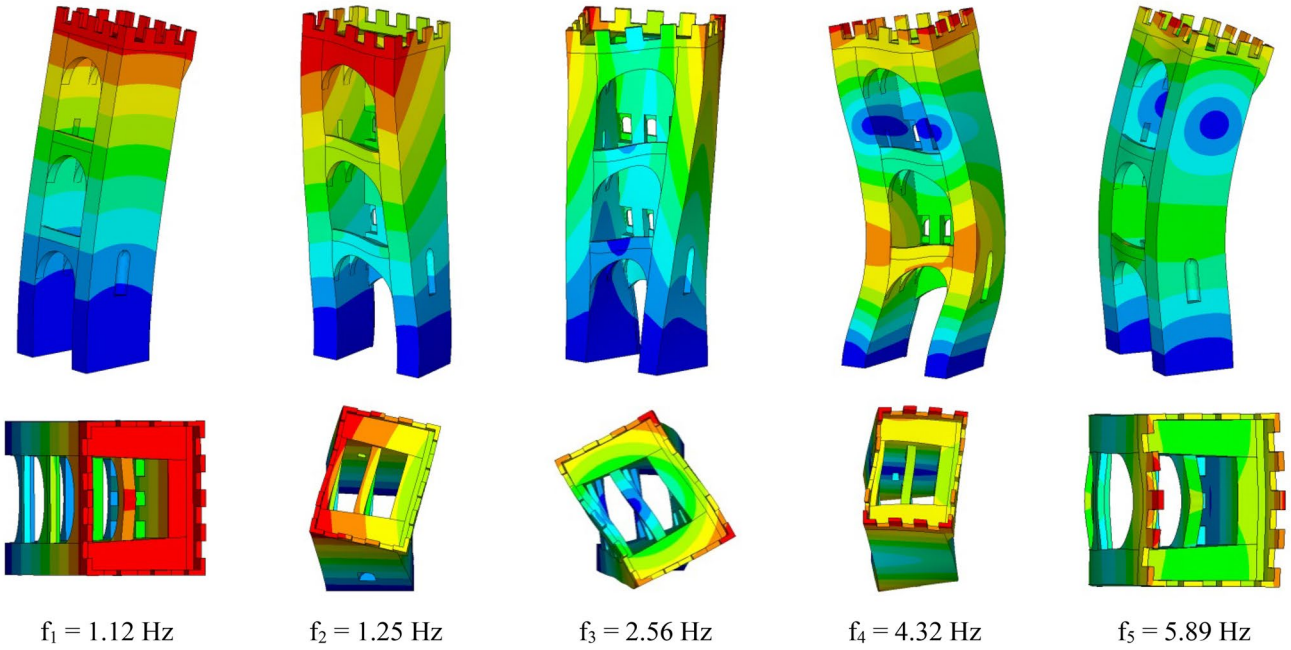

Fig. 10 View of the first 5 mode shapes (FE model with material properties suggested by the code)

dynamic behaviour is highly influenced by the effect of the transversal connection between the two thick walls introduced by the internal masonry arches. Thus, the common assumption of rigid plane behaviour of the levels seems not to be respected, with the walls behaving somewhat independently. This is clearly visible, when analysing the mode shapes, for the torsional modes and the higher bending mode shapes (see Figs. 8 and 9).

it is worth noting, in addition, that if to characterize the (elastic) material properties of the gate the provision suggested by the code [31] were employed (namely $E = 4000$ MPa and $W = 2200$ kg/m^3), the FE model provides values of the frequencies that are considerably underestimated compared to the experimental values. Moreover, the mode shapes (Fig. 10) show an inversion of the first two bending modes with respect to those experimentally assessed (Fig. 7). This result further confirms that this structural typology deserves specific attention from the scientific community and therefore dynamic testing campaigns are strongly recommended to avoid failures in the definition of suitable FE models used to perform a structural assessment.

6 Simulated AV tests

After tuning, the identified FE Model was used as a digital laboratory to simulate the dynamic response of the gate. This virtually allows to collect data with a sensor grid layout more denser than the one that was possible during the experimental campaign (potentially since each node of the FE model can be considered as a possible sensor position, the number of the sensors is equal to the dofs of the model).

A Gaussian white noise was applied, and the acceleration time-histories were acquired according to the layout reported in Fig. 11.

To perform the time-history analyses, a sampling rate of 50 Hz was used to reduce the computational effort and a signal length of 15 s was considered. The simulated AVT were processed in frequency and time domain, as done for the experimental results, to check the modal properties (Table 3). Subsequently, the simulated dynamic signatures were used as a reference to evaluate the optimal reduced sensor grid.

7 Optimal sensor position (OSP)

The simulated AV responses of the tuned FE model allowed to characterize through OMA the modal behaviour of the gate with the reference sensor grid shown in Fig. 11. 8 mono-directional sensors at each level were considered for a total of $N = 24$ possible locations. Since the OSP here investigated is a subset of the reference layout, the minimum number of employed sensors will depend on the number of mode shapes N_m that can be identified. For the sake of clarity, the test was focused on the identification of the first three mode shapes ($N_m = 3$) and consequently as possible positions of the sensors only the last floor is considered (positions from 9 to 12 in Fig. 11) for a total of $N = 8$.

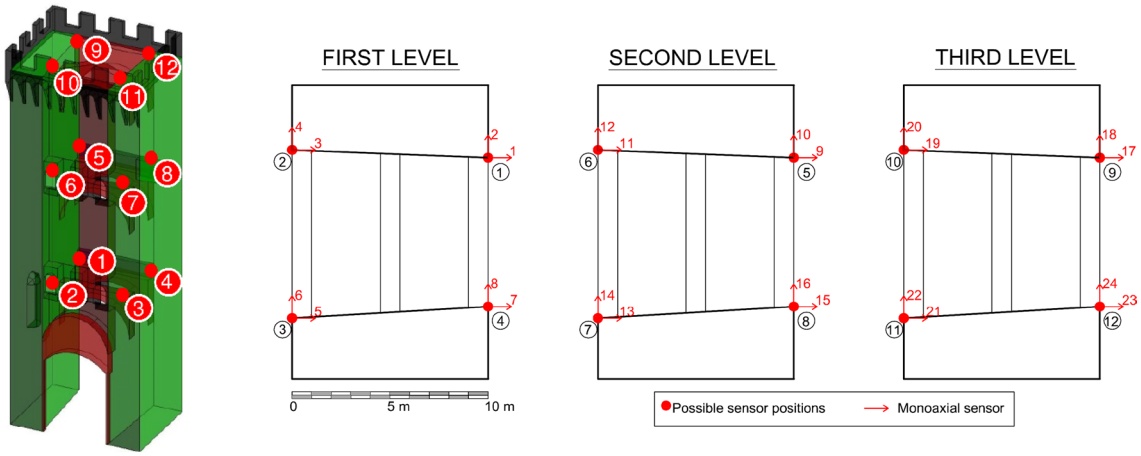

Fig. 11 Possible sensor positions in the gate

The permutations C of the N_s sensors over the reduced system of N dofs can be quantified by the following binomial expansion:

$$C = \begin{pmatrix} N \\ N_s \end{pmatrix} = \frac{N!}{(N - N_s)!N_s!} \tag{2}$$

It is worth noting that if the OSP should be assessed by including also higher mode shapes ($N_m > 3$), the number of the possible combinations C to be investigated would increase abruptly, being necessary to include sensors on the intermediate levels (to identify the higher mode shapes). For instance, include an additional level, means, at least, $N_s = 6$ over $N = 16$ possible positions corresponding to a number of permutations $C = 8008$. If another monitored level is added ($N = 24$ and $N_s = 9$), the number of permutations increases to 1,307,504.

By investigating OSP for only the first three mode shapes ($N_m = 3$), over a reduced set of measurable dofs ($N = 8$), the following cases are considered: (a) In a first case, only three devices at the last floor are considered ($N_s = 3$). Using Eq. (1), the possible combinations of the sensor positions are 56 (see Table 5 in Appendix): 8 of them involve sensors measuring only in one direction, 24 combinations involve a biaxial measuring station, the remaining 24 combinations are composed by monoaxial stations in the two horizontal directions. (b) In a second case the number of devices is increased up to four ($N_s = 4$), to quantify the information added by an extra sensor. In this case, the possible combination raises to 70 (see Table 6 in the Appendix): 6 combinations with two biaxial stations, 46 combinations with at least one biaxial station and 18 combinations with four monoaxial stations.

To approach OSP several methods were introduced by researchers. While in [46] the OSP was tackled minimizing the information entropy that was assumed as a metric of the performance of the sensor configuration, in [47] Kammer proposed a method based on the maximization of the Fisher Information Matrix (FIM). This method is quite straightforward and computationally efficient, thus the method proposed by Kammer in [47], with the enhanced algorithm introduced by Stephan in [48] (Fig. 12), was here adopted as a baseline to solve the OSP.

As shown in Fig. 12, the OSP is tackled by selecting the k-th set of sensors which maximizes, along each direction, the FIM. This matrix I_k, is calculated according to Eq. (2):

$$I_k = \sum_{k=1}^{N_s} I_{\mathrm{el},k} \tag{3}$$

where $I_{\mathrm{el},k}$ denotes the elementary FIM of the k-th sensor position, calculated using the following Eq. (3):

$$I_{\mathrm{el},k} = \phi_k^T \phi_k \tag{4}$$

where ϕ_k, denotes a sub-partition of the modal matrix $\boldsymbol{\Phi} \in \mathbb{R}^{N \times N_m}$, corresponding to the k-th dof where the sensor can be positioned.

To quantify the level of information condensed in the chosen set of sensors, a proper norm must be defined. As suggested in [48], the spectral radius of I_k was here adopted as metric. This allows to identify the sensors that exhibit the highest contribution on the observed mode shapes.

The distribution of $I_{\mathrm{el},i}$ is reported in Fig. 13. It is possible to order the maximum information collected by the sensor positions at the last level as follows: (1) in the x-direction (EW) the sensors 19–21–23–17; (2) in the y-direction (NS) the sensors 22–20–24–18 (see Fig. 11).

Nevertheless, some of these sensors can share the same information without increasing the accuracy of the mode

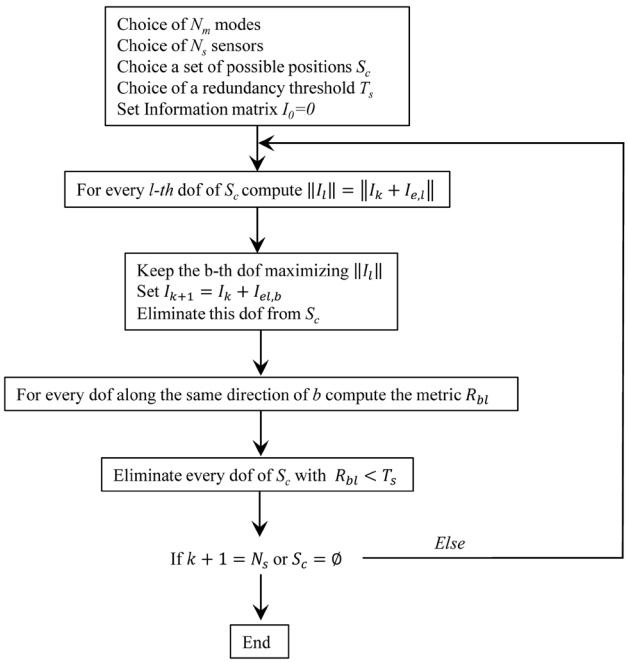

Fig. 12 The flowchart of the algorithm proposed in [48]

shape estimation. Thus, the redundancy between the elementary information matrices of the sensors must be taken into account. This can be done, by considering the following normalized metric R_{kl} between two elementary FIM $I_{\mathrm{el},k}$ and $I_{\mathrm{el},l}$:

$$R_{kl} = \frac{||I_{\mathrm{el},k} - I_{\mathrm{el},l}||}{||I_{\mathrm{el},k} + I_{\mathrm{el},l}||} \tag{5}$$

Finally, the OSP is assessed maximizing the information contents and minimizing the redundancy between each sensor. This means that at each run of the algorithm shown in Fig. 12, the k-th sensor exhibiting the highest contribution to I_k is retained. Then the redundancy R_{kl} with the other l-th sensors along the same direction is assessed.

For instance, in Fig. 14 the results of R_{kl} for the two main directions of San Niccolò gate (measured at the last level), is shown; obviously for $k=l$, the maximum redundancy level is attained ($R_{kl} = 0$), while the lowest ($R_{kl} = 1$) is expected when no information are shared by the sensors.

Stephan in [48] suggests keeping all the sensors above a redundancy threshold equal to 0.5 and I_l is so formed by the sum of the FIM of all the retained sensors and the elementary FIM $I_{\mathrm{el},l}$ the l-th sensor itself.

In this study the way to compute I_l has been modified to consider the influence of the redundancy level as follows:

$$I_l = R_{ln} \sum_{n=1}^{k} I_n + I_{\mathrm{el},l} \tag{6}$$

As a consequence, no thresholds on the redundancy must a-priori be fixed (e.g. $R_{kl} = 0.5$ as in [48]) and all the possible FIM for every set of sensor are evaluated according to Eq. (6). To check the effectiveness of the method, a new coherence index (θ_k) was introduced. For the k-th set of sensors, θ_k computes the average correlation between the mode shapes $\tilde{\phi} \in \mathbb{R}^{N_s \times N_m}$ (those obtained by OSP) and $\phi_0 \in \mathbb{R}^{N \times N_m}$ (those provided by the simulated AVT):

$$\theta_k = \frac{1}{N_m} \sum_{i=1}^{N_m} \mathrm{MAC}\left(\tilde{\phi}_i, \phi_{0i}\right) \tag{7}$$

where $N_m = 3$ still represents the number of the investigated mode shapes.

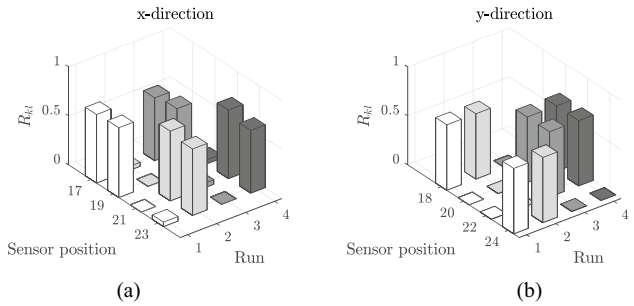

Fig. 14 The redundancy R_{kl} for x (**a**) and y (**b**) direction, at each run

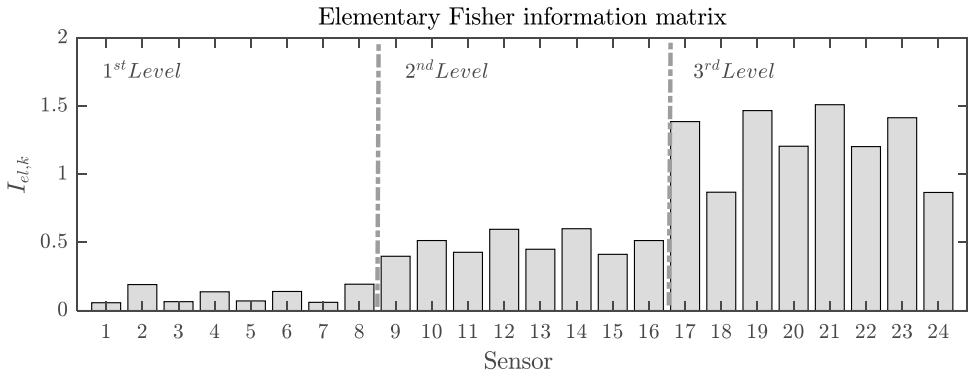

Fig. 13 The norm of the elementary FIM for each sensor position in the observation of the first three mode shapes

It is worth noting that the dimension of $\tilde{\phi}_i$ and ϕ_{0i} is different because not all the dofs are available in $\tilde{\phi}$ since $N > N_s$. Hence the missing values of $\tilde{\phi}$ are replaced with a linear interpolation of the N_s measured values.

When considering the first case (a), where only three devices at the last floor were assumed ($N_s = 3$), the values of the θ_k (Eq. (7)) are reported in Fig. 15a. Only the 14% (see Fig. 15c) of all the possible configurations is able to reach a value higher than 0.9, and major differences can be observed in the estimation of the third mode shape that reach a maximum value of the MAC equal to 0.77 (Fig. 15b).

When the second case is analysed (b), with the number of devices increased up to four ($N_s = 4$), a better estimation of the torsional mode can be observed. Although this is not an unexpected outcome (an additional sensor provides in addition robustness to the SHM system), but, it is worth mentioning that the adoption of this methodology allows for a quantification of the benefits of adopting an additional sensor (or vice versa to estimate what is lost by reducing the number of sensors). With this extra-sensor, an overall improvement of the index θ_k can be observed in Fig. 16a. Highest values are reached with peaks around 0.98 against the 0.92 obtained in the previous case. At least 50% of all the possible combinations stand above 0.90 (as visible in Fig. 16a) with a significant increase in the performance of the system for the third mode shape estimation (see Fig. 16b). The MAC of this mode reaches values above 0.90 (compared to the value of 0.77 obtained for the first case).

The complete list of the best combination obtained for $N_s = 3$ and $N_s = 4$ is reported in Table 4a, b, respectively.

8 Concluding remarks and future outlook

Historical city gates, which are apparently similar to the typology of masonry towers, are what today remains of the defensive structures that characterised the medieval centres of many European cities. Being the surviving gates frequently immersed in the daily vehicular traffic flows and continuously subjected to traffic-induced vibrations, specific studies and research are hence needed to allow their preservation. This paper presented a pilot project for long-term structural health monitoring of historical city gates by discussing a methodology to be adopted for the assessment of the optimal sensor position. The workflow includes four phases: (1) an expeditious dynamic testing aimed to assess the dynamic signature of the city gate; (2) a numerical model updated based on the experimental frequencies which is subsequently (3) employed as a virtual laboratory to simulate ambient vibration tests, and (4) the maximization of the Fisher Information Matrix and the simultaneous minimization of the redundancy between the information matrices of the sensors for the assessment of the optimal sensor position. This workflow, which is aimed at providing a low-cost and sustainable dynamic monitoring system (by maximizing the information collected by a limited number of sensors), allows for an objective quantification of the efficiency of the adopted sensor grid (or, vice versa, to have an estimation of the quantity of information that are lost by reducing the number of sensors). To quantity this information, a coherence index was proposed. For instance, for the case analysed in this paper, it was shown that when considering only three devices only 14% of all the possible configurations is able to reach a coherence index higher than 0.9 (with major differences in the estimation of the third mode shape). With an additional device, at least 50% of all the combinations are higher than 0.90 and the index of the third mode reaches values above 0.90 (compared to the value of 0.77 obtained with only three devices).

However, the above workflow has been proposed in a deterministic model updating framework, thus meaning that it does not account for the uncertainties associated with the experimental measurements and the modelling errors which may lead to false positives identification results.

Table 4 Results of I_l and θ_k for the best combinations, respectively using a set of (a) three and (b) four sensors

(a) Combination	Positions			I_l	θ_k	(b) Combination	Positions				I_l	θ_k
COMB-37	19	20	21	3.77	0.877	COMB-8	17	18	20	23	4.086	0.980
COMB-41	19	21	22	3.77	0.873	COMB-13	17	18	22	23	4.081	0.980
COMB-27	18	20	21	3.29	0.778	COMB-31	17	20	23	24	4.082	0.980
COMB-22	18	19	20	3.25	0.784	COMB-35	17	22	23	24	4.079	0.980
COMB-3	17	18	21	3.34	0.914	COMB-58	19	20	21	24	4.335	0.980
COMB-5	17	18	23	3.17	0.908	COMB-61	19	20	23	24	4.207	0.980
COMB-18	17	21	24	3.35	0.913	COMB-63	19	21	22	24	4.202	0.980
COMB-21	17	23	24	3.17	0.907	COMB-65	19	22	23	24	4.337	0.980
COMB-23	18	19	21	3.42	0.920	COMB-36	18	19	20	21	4.335	0.979
COMB-25	18	19	23	3.29	0.914	COMB-58	19	20	21	24	4.332	0.980
COMB-43	19	21	24	3.41	0.919	COMB-40	18	19	21	22	4.335	0.979
COMB-46	19	23	24	3.29	0.913	COMB-38	18	19	20	23	4.209	0.979

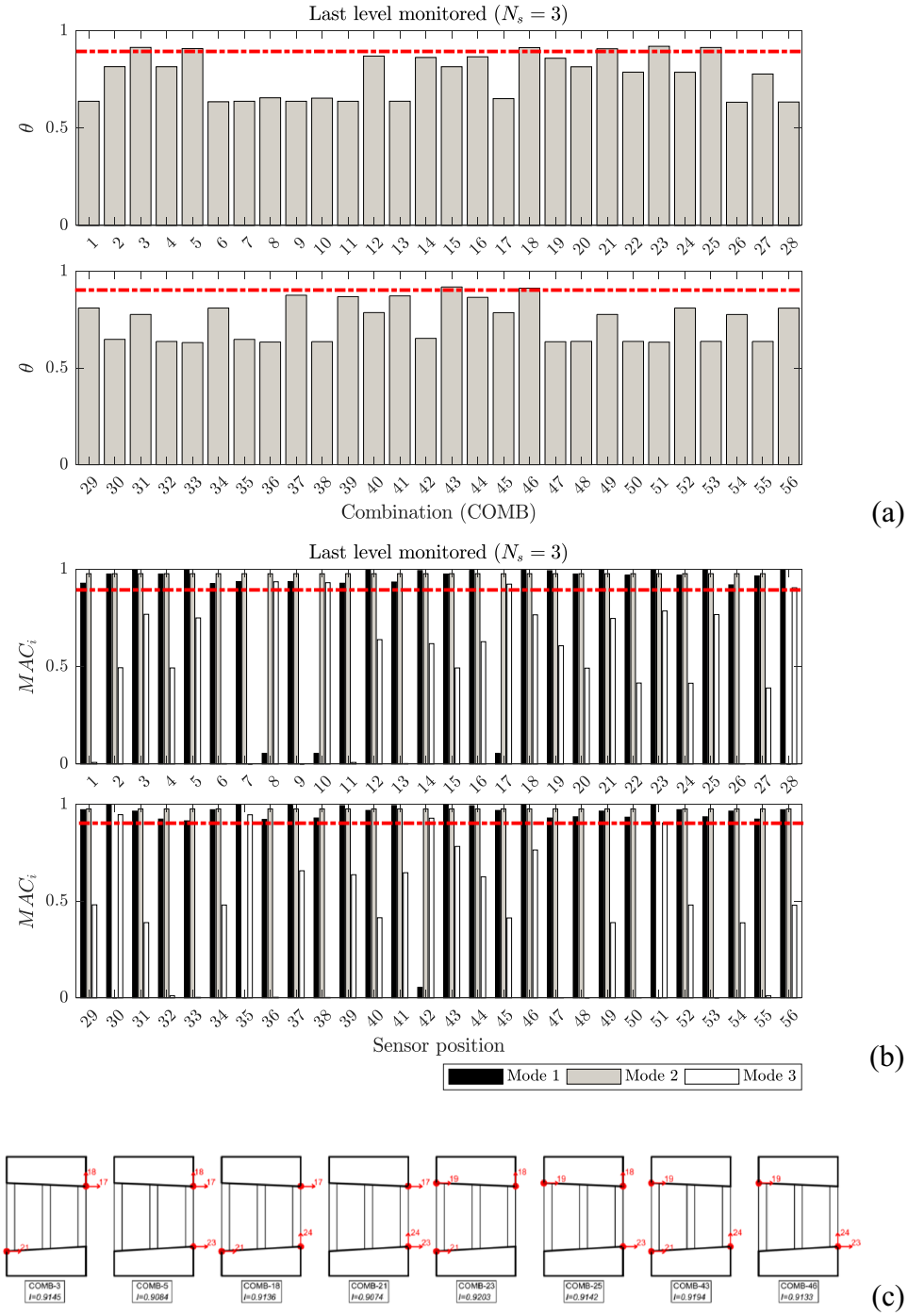

Fig. 15 Results of **a** the I index **b** of each mode **c** the eight best-fit combinations in the case of three sensors ($N_s = 3$) at the last level under the hypothesis of rigid body motion. The red line represents the MAC threshold equal to 0.9

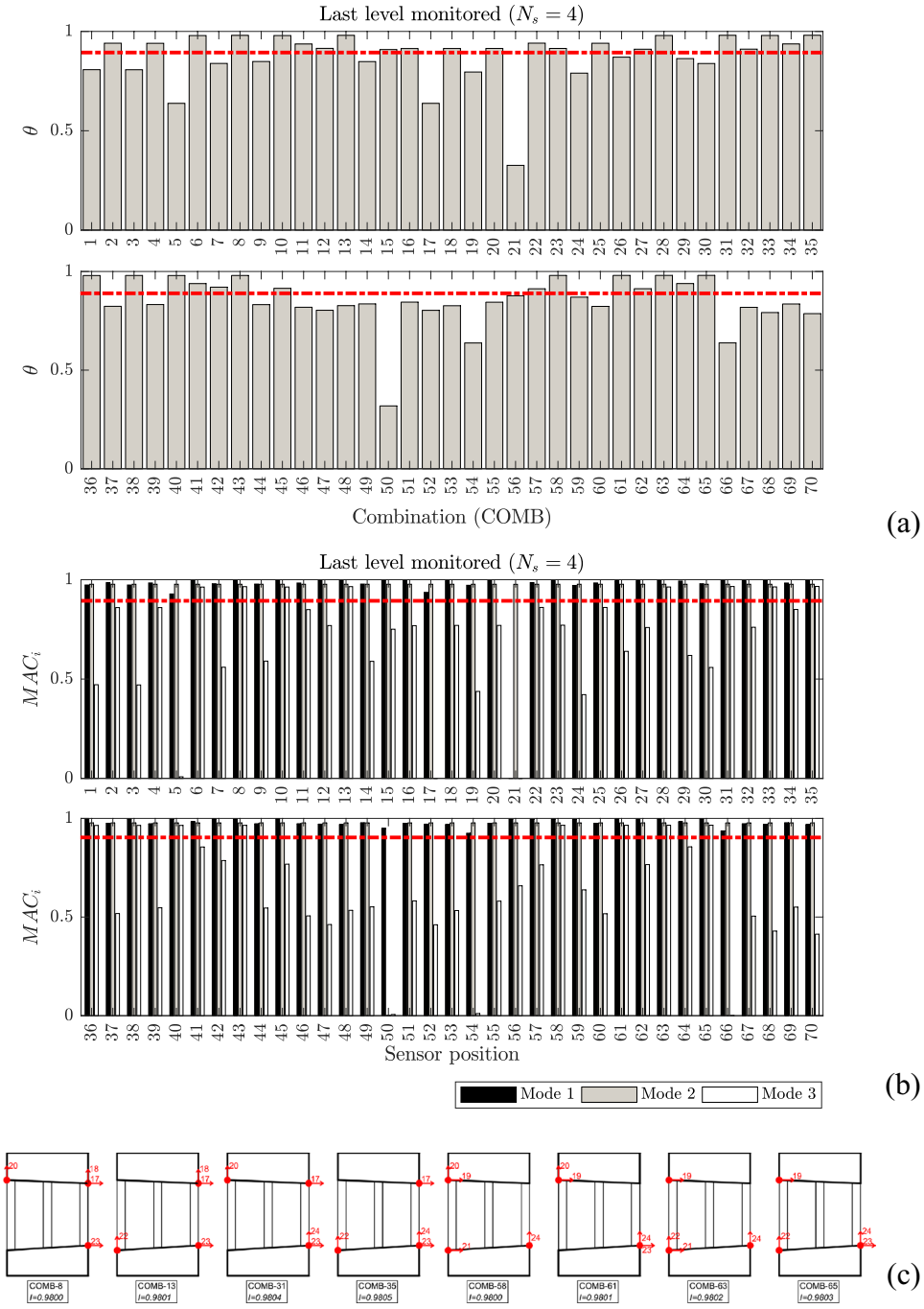

Fig. 16 Results of **a** the *I* index **b** of each mode **c** the eight best-fit combinations in the case of four sensors ($N_s = 4$) at the last level under the hypothesis of rigid body motion (the continuous red line represents the MAC threshold equal to 0.9)

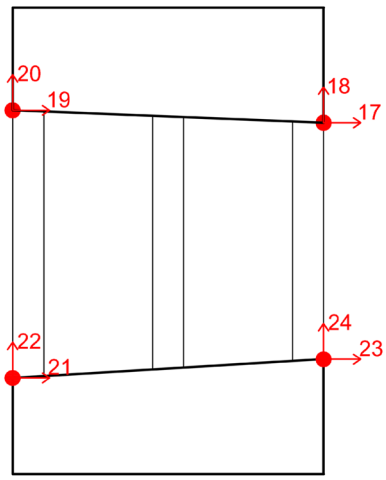

Fig. 17 Possible sensor positions at the last level

Future advances of this study will pay attention to this issue through the Bayesian approach which constitutes an efficient and rigorous mathematical framework to account for the probabilistic modelling of the different sources of uncertainty which affect the system output. Nonetheless, this pilot project aimed at rationalizing the first step required for the sustainable and efficient definition of a long-term monitoring system. It is the opinion of the authors that the methodology (the workflow) proposed in this paper can be generalized and employed in similar cases.

Appendix

In Fig. 17 are reported all the feasible sensor positions at the last level and in Tables 5 and 6 all the possible configurations adopting three or four sensors respectively.

Table 5 All the possible combinations of the sensor positions for $N_s = 3$

Combination	Positions			Combination	Positions		
COMB-1	17	18	19	COMB-29	18	20	23
COMB-2	17	18	20	COMB-30	18	20	24
COMB-3	17	18	21	COMB-31	18	21	22
COMB-4	17	18	22	COMB-32	18	21	23
COMB-5	17	18	23	COMB-33	18	21	24
COMB-6	17	18	24	COMB-34	18	22	23
COMB-7	17	19	20	COMB-35	18	22	24
COMB-8	17	19	21	COMB-36	18	23	24
COMB-9	17	19	22	COMB-37	19	20	21
COMB-10	17	19	23	COMB-38	19	20	22
COMB-11	17	19	24	COMB-39	19	20	23
COMB-12	17	20	21	COMB-40	19	20	24
COMB-13	17	20	22	COMB-41	19	21	22
COMB-14	17	20	23	COMB-42	19	21	23
COMB-15	17	20	24	COMB-43	19	21	24
COMB-16	17	21	22	COMB-44	19	22	23
COMB-17	17	21	23	COMB-45	19	22	24
COMB-18	17	21	24	COMB-46	19	23	24
COMB-19	17	22	23	COMB-47	20	21	22
COMB-20	17	22	24	COMB-48	20	21	23
COMB-21	17	23	24	COMB-49	20	21	24
COMB-22	18	19	20	COMB-50	20	22	23
COMB-23	18	19	21	COMB-51	20	22	24
COMB-24	18	19	22	COMB-52	20	23	24
COMB-25	18	19	23	COMB-53	21	22	23
COMB-26	18	19	24	COMB-54	21	22	24
COMB-27	18	20	21	COMB-55	21	23	24
COMB-28	18	20	22	COMB-56	22	23	24

Table 6 All the possible combinations of the sensor positions for $N_s = 4$

Combination	Positions				Combination	Positions			
COMB-1	17	18	19	20	COMB-36	18	19	20	21
COMB-2	17	18	19	21	COMB-37	18	19	20	22
COMB-3	17	18	19	22	COMB-38	18	19	20	23
COMB-4	17	18	19	23	COMB-39	18	19	20	24
COMB-5	17	18	19	24	COMB-40	18	19	21	22
COMB-6	17	18	20	21	COMB-41	18	19	21	23
COMB-7	17	18	20	22	COMB-42	18	19	21	24
COMB-8	17	18	20	23	COMB-43	18	19	22	23
COMB-9	17	18	20	24	COMB-44	18	19	22	24
COMB-10	17	18	21	22	COMB-45	18	19	23	24
COMB-11	17	18	21	23	COMB-46	18	20	21	22
COMB-12	17	18	21	24	COMB-47	18	20	21	23
COMB-13	17	18	22	23	COMB-48	18	20	21	24
COMB-14	17	18	22	24	COMB-49	18	20	22	23
COMB-15	17	18	23	24	COMB-50	18	20	22	24
COMB-16	17	19	20	21	COMB-51	18	20	23	24
COMB-17	17	19	20	22	COMB-52	18	21	22	23
COMB-18	17	19	20	23	COMB-53	18	21	22	24
COMB-19	17	19	20	24	COMB-54	18	21	23	24
COMB-20	17	19	21	24	COMB-55	18	22	23	24
COMB-21	17	19	21	23	COMB-56	19	20	21	22
COMB-22	17	19	21	24	COMB-57	19	20	21	23
COMB-23	17	19	22	23	COMB-58	19	20	21	24
COMB-24	17	19	22	24	COMB-59	19	20	22	23
COMB-25	17	19	23	24	COMB-60	19	20	22	24
COMB-26	17	20	21	22	COMB-61	19	20	23	24
COMB-27	17	20	21	23	COMB-62	19	21	22	23
COMB-28	17	20	21	24	COMB-63	19	21	22	24
COMB-29	17	20	22	23	COMB-64	19	21	23	24
COMB-30	17	20	22	24	COMB-65	19	22	23	24
COMB-31	17	20	23	24	COMB-66	20	21	22	23
COMB-32	17	21	22	23	COMB-67	20	21	22	24
COMB-33	17	21	22	24	COMB-68	20	21	23	24
COMB-34	17	21	23	24	COMB-69	20	22	23	24
COMB-35	17	22	23	24	COMB-70	21	22	23	24

Acknowledgements The authors acknowledge the municipality of Florence for the availability in carrying out the experimental tests.

References

1. Sepe V, Speranza E, Viskovic A (2008) A method for large-scale vulnerability assessment of historic towers. Struct Control Health Monit 15:389–415. https://doi.org/10.1002/stc.243
2. Casolo S, Milani G, Uva G, Alessandri C (2013) Comparative seismic vulnerability analysis on ten masonry towers in the coastal Po Valley in Italy. Eng Struct 49:465–490. https://doi.org/10.1016/j.engstruct.2012.11.033
3. Anzani A, Binda L, Carpinteri A, Invernizzi S, Lacidogna G (2010) A multilevel approach for the damage assessment of Historic masonry towers. J Cult Herit 11:459–470. https://doi.org/10.1016/j.culher.2009.11.008
4. Bartoli G, Betti M, Monchetti S (2017) Seismic risk assessment of historic masonry towers: comparison of four case studies. ASCE's J Perform Construct Facil 31(5):04017039. https://doi.org/10.1061/(ASCE)CF.1943-5509.0001039

5. Ivorra S, Giannoccaro NI, Foti D (2019) Simple model for predicting the vibration transmission of a squat masonry tower by base forced vibrations. Struct Control Health Monit 26:e2360. https://doi.org/10.1002/stc.2360
6. Bennati S, Nardini L, Salvatore W (2005) Dynamic behavior of a medieval masonry bell tower. II: Measurement and modeling of the tower motion. J Struct Eng 131(11):1656–1664. https://doi.org/10.1061/(ASCE)0733-9445(2005)131:11(1656)
7. Bru D, Ivorra S, Betti M, Adam JM, Bartoli G (2019) Parametric dynamic interaction assessment between bells and supporting slender masonry tower. Mech Syst Signal Process 129:235–249. https://doi.org/10.1016/j.ymssp.2019.04.038
8. Barsocchi P, Cassara P, Mavilia F, Pellegrini D (2018) Sensing a city's state of health: structural monitoring system by internet-of-things wireless sensing devices. IEEE Consumer Electron Mag 7:2–31. https://doi.org/10.1109/MCE.2017.2717198
9. Barsocchi P, Bartoli G, Betti M, Girardi M, Mammolito S, Pellegrini D, Zini G (2021) Wireless sensor networks for continuous structural health monitoring of historic masonry towers. Int J Arch Herit 15(1):22–44. https://doi.org/10.1080/15583058.2020.1719229
10. Zonta D, Wu H, Pozzi M, Zanon P, Ceriotti M, Mottola L, Picco GP, Murphy AL, Guna S, Corra M (2010) Wireless sensor networks for permanent health monitoring of historic buildings. Smart Struct Syst 6(5):595–618. https://doi.org/10.1298/sss.2010.6.5_6.595
11. Saisi A, Gentile C (2015) Post-earthquake diagnostic investigation of a historic masonry tower. J Cult Herit 16:602–609. https://doi.org/10.1016/j.culher.2014.09.002
12. Saisi A, Gentile C, Ruccolo A (2018) Continuous monitoring of a challenging heritage tower in Monza, Italy. J Civ Struct Heal Monit 8:77–90. https://doi.org/10.1007/s13349-017-0260-5
13. Cavalagli N, Comanducci G, Gentile C, Guidobaldi M, Saisi A, Ubertini F (2017) Detecting earthquake-induced damage in historic masonry towers using continuously monitored dynamic response-only data. Procedia Eng 199:3416–3421. https://doi.org/10.1016/j.proeng.2017.09.581
14. Gentile C, Guidobaldi M, Saisi A (2016) One-year dynamic monitoring of a historic tower: damage detection under changing environment. Meccanica 51(11):2873–2889. https://doi.org/10.1007/s11012-016-0482-3
15. Ubertini F, Comanducci G, Cavalagli N (2016) Vibration-based structural health monitoring of a historic bell–tower using output-only measurements and multivariate statistical analysis. Struct Health Monit 15(4):438–457. https://doi.org/10.1177/1475921716643948
16. Ubertini F, Cavalagli N, Kita A, Comanducci G (2018) Assessment of a monumental masonry bell-tower after 2016 Central Italy seismic sequence by long-term SHM. Bull Earthq Eng 16:775–801. https://doi.org/10.1007/s10518-017-0222-7
17. Garcia-Macias E, Ierimonti L, Venanzi I, Ubertini F (2021) An innovative methodology for online surrogate-based model updating of historic buildings using monitoring data. Int J Arch Herit 15(1):92–112. https://doi.org/10.1080/15583058.2019.1668495
18. Ubertini F, Gentile C, Materazzi AL (2013) Automated modal identification in operational conditions and its application to bridges. Eng Struct 46:264–278. https://doi.org/10.1016/j.engstruct.2012.07.031
19. Zini G, Betti M, Bartoli G (2022) A quality-based automated procedure for operational modal analysis. Mech Syst Signal Process 164:108173. https://doi.org/10.1016/j.ymssp.2021.108173
20. Pallarés FJ, Betti M, Bartoli G, Pallarés L (2021) Structural health monitoring (SHM) and Nondestructive testing (NDT) of slender masonry structures: a practical review. Constr Build Mater 279:123768. https://doi.org/10.1016/j.conbuildmat.2021.123768
21. Zonta D, Pozzi M, Zanon P (2008) Managing the historical heritage using distributed technologies. Int J Arch Herit 2(3):200–225. https://doi.org/10.1080/15583050802063691
22. Ceriotti M, Mottola L, Picco GP, Murphy AL, Guna S, Corrà M, Pozzi M, Zonta D, Zanon P (2009) Monitoring heritage buildings with wireless sensor networks: the torre aquila. In: Proceedings of the 8th international conference on information processing in sensor networks, San Francisco, USA
23. Crispino M, D'Apuzzo M (2001) Measurement and prediction of traffic-induced vibrations in a heritage building. J Sound Vib 246:319–335. https://doi.org/10.1006/jsvi.2001.3648
24. Fratini M, Pieraccini M, Atzeni C, Betti M, Bartoli G (2011) Assessment of vibration reduction on the Baptistery of San Giovanni in Florence (Italy) after vehicular traffic block. J Cult Herit 12:323–328. https://doi.org/10.1016/j.culher.2011.01.003
25. Baraccani S, Azzara RM, Palermo M, Gasparini G, Trombetti T (2020) Long-term seismometric monitoring of the two towers of bologna (Italy): modal frequencies identification and effects due to traffic induced vibrations, Front. Built Environ 6:1–14. https://doi.org/10.3389/fbuil.2020.00085
26. Zini G, Betti M, Bartoli G (2022) Experimental analysis of the traffic-induced-vibration on an ancient lodge. Struct Control Health Monit 29:e2900. https://doi.org/10.1002/stc.2900
27. Cabboi A, Magalhães F, Gentile C, Cunha Á (2017) Automated modal identification and tracking: application to an iron arch bridge. Struct Control Health Monit 24:e1854. https://doi.org/10.1002/stc.1854
28. Rainieri C, Fabbrocino G (2015) Development and validation of an automated operational modal analysis algorithm for vibration-based monitoring and tensile load estimation. Mech Syst Signal Process 60:512–534. https://doi.org/10.1016/j.ymssp.2015.01.019
29. Lourenço PB (2002) Computations of historical masonry constructions. Prog Struct Eng Mater 4(3):301–319. https://doi.org/10.1002/pse.120
30. Betti M, Galano L, Vignoli A (2016) Earthquakes and their impact on society. Springer, Cham, pp 377–415. https://doi.org/10.1007/978-3-319-21753-6_14
31. NTC2008 (2008) Nuove Norme Tecniche per le Costruzioni. D.M. del Ministero delle Infrastrutture e dei Trasporti del 14/01/2008. G.U. n. 29 del 04.02.2008, S.O. n. 30 **(in Italian)**
32. Faccio P, Podestà S, Saetta A (2009) Venezia, Campanile della Chiesa di Sant'Antonio, Esempio 5." In: Linee guida per la valutazione e riduzione del Rischio Sismico del Patrimonio Culturale Allineate alle Nuove Norme Tecniche per le Costruzioni (DM 14/01/2008) **(in Italian)**
33. NCSE2002 (2002) Norma de Construcciòn Sismorresistente—parte General y Edificaciòn (Spanish Standard). Ministerio de Fomento (in Spanish), Spain
34. Rainieri C, Fabbrocino G (2012) Estimating the elastic period of masonry towers. In: Proceedings of the SEM IMAC 30th conference, society for experimental mechanics Inc., Jacksonville
35. Shakya M, Varum H, Vicente R, Costa A (2014) Empirical formulation for estimating the fundamental frequency of slender masonry structures. Int J Architect Herit 10(1):55–66. https://doi.org/10.1080/15583058.2014.951796
36. Bartoli G, Betti M, Marra AM, Monchetti S (2017) Semiempirical formulations for estimating the main frequency of slender masonry towers. ASCE's J Perform Construct Facil 31(4):04017025. https://doi.org/10.1061/(ASCE)CF.1943-5509.0001017
37. Mottershead JE, Friswell MI (1993) Model updating in structural dynamics: a survey. J Sound Vib 167(2):347–375. https://doi.org/10.1006/jsvi.1993.1340

38. Holland JH (1975) Adaptation in natural and artificial systems. MIT Press, Cambridge
39. Mares C, Surace C (1996) An application of genetic algorithms to identify damage in elastic structures. J Sound Vib 195(2):195–215. https://doi.org/10.1006/jsvi.1996.0416
40. Faravelli L, Materazzi F, Rarina M (2005) Genetic algorithms for structural identification. In: Proceedings of ICOSSAR 2005, Roma, Italy
41. Betti M, Facchini L, Biagini P (2015) Damage detection on a three-storey steel frame using artificial neural networks and genetic algorithms. Meccanica 50:875–886. https://doi.org/10.1007/s11012-014-0085-9
42. Perera R, Ruiz A (2008) A multistage FE updating procedure for damage identification in large-scale structures based on multiobjective evolutionary optimization. Mech Syst Signal Process 22(4):970–991. https://doi.org/10.1016/j.ymssp.2007.10.004
43. Lacanna G, Betti M, Ripete M, Bartoli G (2020) Dynamic identification as a tool to constrain numerical models for structural analysis of historical buildings. Front Built Environ Earthq Eng 6:40. https://doi.org/10.3389/fbuil.2020.00040
44. Shabbir F, Omenzetter P (2016) Model updating using genetic algorithms with sequential-niche technique. Eng Struct 120:166–182. https://doi.org/10.1016/j.engstruct.2016.04.028
45. Boschi S, Galano L, Vignoli A (2019) Mechanical characterisation of Tuscany masonry typologies by in situ tests. Bull Earthq Eng 17:413–438. https://doi.org/10.1007/s10518-018-0451-4
46. Papadimitriou C (2004) Optimal sensor placement methodology for parametric identification of structural systems. J Sound Vib 278:923–947. https://doi.org/10.1016/j.jsv.2003.10.063
47. Kammer DC (1991) Sensor placement for on-iOrbit modal identification and correlation of large space structures. J Guid. https://doi.org/10.2514/3.20635
48. Stephan C (2012) Sensor placement for modal identification. Mech Syst Signal Process 27:461–470. https://doi.org/10.1016/j.ymssp.2011.07.022